Phase-Gradient Huygens' Metasurface Coatings for Dynamic Beamforming in Linear Antennas

Stefano Vellucci, *Member, IEEE*, Michela Longhi, *Member, IEEE*, Alessio Monti, *Senior Member, IEEE*, Mirko Barbuto, *Senior Member, IEEE*, Alessandro Toscano, *Senior Member, IEEE*, and Filiberto Bilotti, *Fellow, IEEE*

***Abstract*— The beamforming capabilities of conformal cylindrical Huygens metasurface (HMS) coatings for linear antennas are assessed. It is shown that by engineering the phase-gradient profile of the HMS, the original omnidirectional radiation pattern of the linear antenna can be shaped to form multi or single-beam configurations. A closed-form expression for the phase-insertion profile of the cylindrical coating required to achieve the desired radiation pattern profile is derived, and several full-wave numerical examples supporting our claims are reported. A configuration exploiting a realistic HMS layout is also discussed and it is shown that by making the metasurface reconfigurable through the use of tunable lumped elements, the radiated beams can be dynamically steered in space. This new design methodology could find application in smart electromagnetic (EM) environment scenarios for dynamically rerouting the signal toward multiple users.**

***Index Terms*— 6G, beamforming, Huygens, linear antenna, metasurfaces, radiation pattern, reconfigurable, smart electromagnetic (EM) environment.**

I. Introduction

WIRELESS systems for next-generation communications (e.g., B5G, 5G+, 6G) will face more stringent requirements compared to the current standard, relying on an increased number of connections, expanded user density, higher data transfer, lower latency, almost zero jitters, broadband connectivity, and massive reliability [1], [2]. Since these key performance indicators (KPIs) should be achieved while retaining low costs and minimum infrastructure complexity [3], [4], communication schemes exploiting carriers at sub-6 GHz and millimeter wave frequencies are expected to be the key pillar of future wireless services [5], [6]. Still, with the increase of the operative frequencies, the KPIs achievement is challenged by several detrimental factors due to the environment. Among them, path loss, blockage, and undesired scattering threaten the link budget in both outdoor and indoor scenarios. Unfortunately, attenuation experienced by the signals becomes severe at higher frequencies and countermeasures able to guarantee a stable and reliable quality of service are mandatory [7], [8]. Indeed, conventional solutions exploited in previous wireless communications generations, such as the network densification through an increase in the number of base-stations (BTS) or the boost of the antennas' effective isotropic radiated power (EIRP), are not preferred solutions due to the cost increase, massive power consumption, and alarming electromagnetic field (EMF) levels [9], [10]. A paradigm change, thus, is required through a modification of the communication scheme.

A promising solution to address these issues relies on the concept of a *smart electromagnetic*(EM) *environment* [11], [12], [13], [14], [15], [16], [17], [18]. In this framework, the environment is exploited as a new degree of freedom in the design of the communication scheme, rather than an impairment, and the propagation scenario plays a core role in mitigating losses, distortion, and fading of the EM waves. This new paradigm is enabled by the development of different design strategies and innovative technologies, which introduce elements with "smartness" embedded at the physical layer, without requiring time-consuming and high-latency post-processing of network virtualized functions (NTFs) [19].

Toward this end, a first successful example can be found in the so-called *smart skins* [14], [20], [21], which are static and low-cost metasurfaces that allow for a judicious manipulation of the reflected EM waves, even out of the classical Snell's laws, for covering spots and improve the non-line-of-sight performance. The feasibility of this solution is however paid with the absence of reconfigurable capabilities that limits their range of applications. To overcome this limitation, recently, extensive research efforts have been focused on the design of *reconfigurable-intelligent surfaces* (RISs) [12], [18], [22], [23], [24], [25], [26]. Such a technology exploits engineered metasurfaces covering buildings, walls, etc., that are made reconfigurable by means of electronic components. In this way, the incoming EM waves can be adaptively reflected toward anomalous angles. The tunability of the reflected wave's direction allows for easy beam management, making RISs a powerful tool to expand the channel capacity. Still, the presence of electronic components requires

Manuscript received 8 February 2023; revised 16 May 2023; accepted 12 July 2023. Date of publication 25 July 2023; date of current version 6 October 2023. This work was supported in part by the activities of the Project MANTLES and in part by the Italian Ministry of University and Research through PRIN 2017 Program under Protocol 2017BHFZKH. *(Corresponding author: Stefano Vellucci.)*

Stefano Vellucci, Michela Longhi, and Mirko Barbuto are with the Department of Engineering, Niccolò Cusano University, 00166 Rome, Italy (e-mail: stefano.vellucci@unicusano.it).

Alessio Monti, Alessandro Toscano, and Filiberto Bilotti are with the Department of Industrial, Electronic and Mechanical Engineering, Roma Tre University, 00154 Rome, Italy.

Color versions of one or more figures in this article are available at https://doi.org/10.1109/TAP.2023.3297193.

Digital Object Identifier 10.1109/TAP.2023.3297193

highly performing manufacturing, increased installation costs, and proper power management.

Finally, to further assist the smartness of the communication scheme, *smart repeaters*and *antennas* with dynamic amplification and forward control capability are introduced in the smart EM environment scenario [27]. These higher-level smart nodes are expected to further enhance the coverage capability of the network, boosting the signal strength, and introducing reconfigurable retransmission capabilities. Compared to current technologies, where the repeaters are characterized by an omni or fixed directionality, i.e., having transmission and reception characteristics fixed over time, next-generation smart antennas will require multibeam capability and adaptability to maximize the data link performance with the final user [19] in both outdoor and indoor scenarios. Thus, antenna solutions introducing reconfigurability and shaping of the radiation pattern, scattering manipulation, and/or tuning of the frequency of operation may be profitably considered.

In this general context, a class of antennas covered by conformal and flexible metasurface sheets enabling advanced control over scattering and electrical characteristics has been proposed in the last decade [28], [29]. In these cases, the metasurface is used as a shell wrapped around a linear antenna introducing advanced wave-manipulation functionalities, albeit allowing for proper reception/transmission of the incoming signal (i.e., not isolating the antenna from the surrounding environment). For instance, one of the first devices exploiting this design strategy relies on the use of coating metasurfaces for cloaking functionalities. In this scenario, the metasurface coating is used to suppress the fundamental scattering mode of the antenna, minimizing its visibility level. Thanks to the typically electrically thin radius of filar antennas, scattering cancellation principles [30] can be efficiently applied by means of a metasurface specifically designed to reradiate a field out-of-phase with the field scattered by the antenna itself [31]. Hence, achieving an invisibility effect and enabling the design of extremely compact telecommunication platforms equipped with multiple antenna systems confined in a reduced space [32], [33], [34], [35], [36]. Remarkably, the applications enabled by conformal cloaking metasurfaces have been even more expanded by utilizing non-linear electronic devices loading the metasurface and conceiving antennas and array systems exhibiting different radiation characteristics depending on the power level or even the signal waveform [37], [38], [39], [40], [41]. Finally, conformal metasurface shells have been also used for broadening or tuning the antenna's resonance frequency by a judicious variation of the wrapping metasurface response [42], [43], [44]. Compared to the previous approach, here, the wrapping metasurface is engineered to induce secondary currents onto the antenna, hence, perturbing the fundamental resonant mode and enabling the design of frequency-agile systems by equipping the metasurface with varactor diodes [44].

In this contribution, we aim to further expand the potentialities of metasurface shells coating wired antennas and being able to manipulate their scattering, frequency, or radiative characteristics. Namely, the latter application case scenario is here for the first time introduced and discussed, showing how it is possible to manipulate the radiation properties of a linear antenna wrapped by a cylindrical Huygens metasurface (HMS). Thanks to the engineering of the phase-insertion introduced by the phase-gradient discontinuity exhibited by the HMS, the radiation pattern of the antenna is shaped at will on the azimuthal plane. By tuning the surface impedance values of the HMS, i.e., by modifying the phase-gradient profile, beamforming capability is thus introduced. A realistic HMS loaded with varactor diodes is then designed, enabling dynamic control over the radiation beam characteristics.

The article is organized as follows: in Section II, the theory and working principle for achieving beam manipulation are presented, and the analytical formulation for evaluating the phase-insertion profile to be introduced by the gradient HMS is derived. The strategy for discretizing the metasurface depending on the desired radiation pattern shape is also discussed, as well as a complete design workflow for the unit-cells composing the HMS is introduced. In Section III, these design principles are applied to several numerical examples exploiting ideal HMS cells, showing potentialities and limitations of the proposed approach in obtaining single- or multibeam configurations. Finally, in Section IV, we report the design of a realistic configuration made of a reconfigurable HMS loaded with varactor diodes enabling unprecedented dynamic beam-forming capabilities for wire antenna systems.

II. Design Principles of the Cylindrical HMS Coating

In this section, we introduce the use of a cylindrical HMS coating to manipulate the radiation pattern of a linear antenna. Albeit their simplicity, wired antennas such as dipoles, monopoles, strips, etc. are widely used in many applications (e.g., mobile communications, networking, sensing, the Internet of Things (IoT), etc.) because of their straightforward implementation, ease of fabrication, and low cost [45]. Nevertheless, the low directivity and omnidirectionality of the radiation pattern on the H-plane (i.e., on the plane orthogonal to the wire direction) severely limit their range of applications. Hence, augmented linear antennas overcoming this limitation can be particularly appealing to antenna engineers, limiting the use of antenna arrays.

In this framework, recently, HMSs have shown remarkable possibilities in tailoring the EM wavefront. HMSs consist of unit-cells that guarantee the full transmission of the impinging field and full control over its phase through a proper combination of the electric and magnetic dipole moments [46], [47], [48]. The possibility to excite both the dipole moments and properly balance them distinguishes HMSs from conventional metasurfaces, where usually the control of either the electric or magnetic responses is not simultaneous [49]. Indeed, in HMSs, the possibility of properly tailoring the electric and magnetic polarizabilities (or impedances) allows for a peculiar unidirectional radiation pattern. Intriguingly, the name "Huygens" stems from the perpendicular colocation of the electric and dipole moments, which allow to excite currents onto the discontinuity acting as

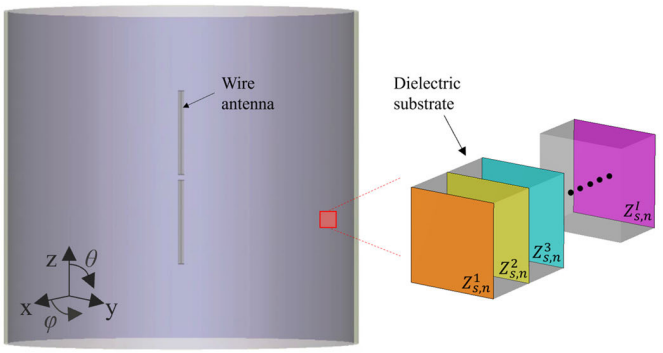

Fig. 1. Reference geometry considered in the article consisting of a cylindrical phase-gradient HMS coating a linear dipole antenna. Through the engineering of the phase gradient introduced by the HMS, beam-steering capabilities are introduced. In the inset, a sketch of the unit-cell configuration used to implement the HMS is reported.

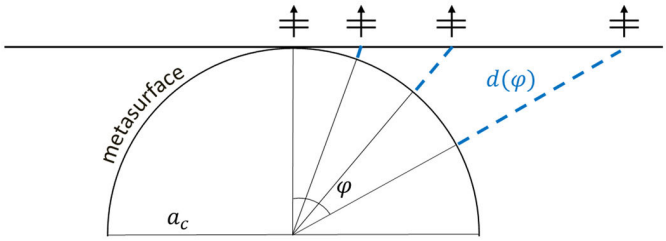

Fig. 2. Schematic representation on a 2-D plane depicting the working principle of the cylindrical HMS. Radial propagation from the central source element is assumed. At the cylindrical discontinuity, the HMS introduces a phase insertion able to compensate for the different electrical paths of the rays $d(\varphi)$ (blue dashed lines) when focused to propagate toward the same direction. The original cylindrical phase-fronts are thus transformed into plane waves. φ represents the angular position of the radiated ray.

secondary unidirectional sources, as envisioned in the Huygens principle [50].

Among the different possibilities enabled by HMSs, the design of phase-gradient metasurfaces for refracting in unconventional ways the incident field is one of the most discussed [51], [52]. In the antenna framework, these platforms have been especially used in phased array scenarios to introduce abrupt discontinuities in the phase of the propagating wave and attain interesting focusing or steering functionalities [53], [54], [55], [56], [57].

However, the steering and beamforming capabilities of phase-gradient HMSs can be extended also to the case of a single radiating source, as recently envisioned in our conference contribution [58]. In Fig. 1, the reference geometry considered here is reported. A conventional half-wavelength dipole antenna is surrounded by a conformal cylindrical HMS of radius a_c, which is designed to introduce a phase-gradient on the *azimuth* direction. Hence, the HMS consists of an anisotropic transition sheet with inhomogeneous unit-cell along the azimuth that aims at manipulating the original omnidirectional pattern of the antenna on the H-plane. Namely, a distributed phase-insertion on the *xoy*-plane is introduced, leading to a focusing effect and beamforming capabilities on the azimuth.

To better explain this point, a half vertical cross section of the problem under consideration is reported in Fig. 2. According to the antenna theory [45], on the azimuthal plane, the phase front of the field radiated by the dipole is (*quasi*-) cylindrical, with a constant value of the phase along the cylindrical profile of the HMS coat. Therefore, at the HMS discontinuity, we have a stable value of the phase of the incoming wave point by point. To achieve the beamforming functionality, the HMS should tailor its phase-insertion by transforming the almost cylindrical wavefront on the horizontal plane into almost planar wavefronts. From Fig. 2, assuming a ray approach and radial propagation, it can be inferred that the HMS should compensate for the different electrical paths of the rays traveling from the omnidirectional source placed at the center. The engineered phase-insertion along the curvilinear profile that leads to the plane wave propagation can be calculated by using elementary trigonometric relations. In particular, the phase-gradient of the HMS assumes the following expression:

$$\Phi(\varphi) = \Phi_0 + k_0 d(\varphi) = \Phi_0 + k_0 a_c \left[1 - \cos^{-1}\varphi\right] \qquad (1)$$

where φ is the geometrical coordinate along the cylindrical profile, Φ_0 is an arbitrary reference phase value, $k_0 = 2\pi/\lambda_0$ is the free-space wavenumber, and $d(\varphi)$ is the differential electrical path of the ray. It is worth noting that to introduce a focusing effect, the phase-insertion $\Phi(\varphi)$ should be an even function. In other terms, the HMS introduces the same phase-insertion for positive and negative values of φ.

Arguably, the number of radiation beams generated exploiting this approach is regulated by the spatial periodicity of the phase-insertion function $\Phi(\varphi)$, which defines the number of sectors into which the HMS is divided, and where a periodicity of 2π corresponds to the full spatial coverage of the circular profile. Due to the symmetry of the problem and the even nature of $\Phi(\varphi)$, the largest periodicity value of the phase-insertion function is π. In this case, the same phase-gradient profile is distributed along a semicircle (as in the scenario in Fig. 2), leading to a two sectors configuration and two main symmetrical radiating beams pointing at opposite directions. Indeed, this point and full-wave numerical results supporting our claim will be better discussed in Section III.

Once the profile of the continuous phase function $\Phi(\varphi)$ is derived, for practical implementation it needs to be discretized in a finite number of samples. Each discrete sample of the function corresponds to a unit-cell of the phase-gradient HMS and we assume a plane-wave impinging onto each cell. Thus, once the number (i.e., $2N-1$) of unit-cells implementing one period of $\Phi(\varphi)$ is fixed, the required phase-insertion $\Phi(\varphi_n)$ exhibited by the nth unit-cell can be derived using (1) (with $n = 1, 2, \ldots, N$).

For the design of the cells exhibiting the required $\Phi(\varphi_n)$, the configuration reported in the inset of Fig. 1 can be considered. Each cell is made of stacked ideal impedance sheets, characterized by a surface impedance value $Z^i_{s,n}$ with $i = 1, 2, \ldots, I$, being I equal to the number of stacked layers. The impedance sheets are separated by the same dielectric substrate of thickness t and relative permittivity ε_r, and the $Z^i_{s,n}$ is assumed to be purely reactive (i.e., $Z^i_{s,n} = jX^i_{s,n}$ with j being the imaginary unit). This configuration enables the excitation of both the electric and magnetic dipole moments ensuring, ideally, high transmission values and a phase coverage that strongly depends on the dielectric thickness [59]. It is worth mentioning that, albeit two impedance sheets are generally enough to design an HMS cell [46], more layers are here considered to increase the phase coverage and the design degrees of freedom.

This stacked configuration can be modeled through a cascade of transmission matrices corresponding to the ABCD matrices of the different material layers and of the transition sheets [61]. Thus, the overall ABCD matrix of the nth unit-cell can be written as

$$\begin{pmatrix} A_n & B_n \\ C_n & D_n \end{pmatrix} = \boldsymbol{Y}^1_{s,n} \cdot \boldsymbol{d} \cdot \boldsymbol{Y}^2_{s,n} \cdot \boldsymbol{d}, \ldots, \boldsymbol{Y}^I_{s,n} \tag{2}$$

where $\boldsymbol{Y}^i_{s,n}$ and $\boldsymbol{d}$ are the ABCD matrices of the admittance sheets and the dielectric substrates, respectively. For normal incidence, the latter reduces to [61] and [62]

$$\boldsymbol{d} = \begin{pmatrix} \cos\left(k_0 d\sqrt{\varepsilon_r}\right) & j\dfrac{\eta_0 \sin\left(k_0 d\sqrt{\varepsilon_r}\right)}{\sqrt{\varepsilon_r}} \\ j\dfrac{\eta_0 \sin\left(k_0 d\sqrt{\varepsilon_r}\right)}{\sqrt{\varepsilon_r}} & \cos\left(k_0 d\sqrt{\varepsilon_r}\right) \end{pmatrix} \tag{3}$$

with η_0 being the free-space wave impedance. If we also assume that the admittance sheets exhibit only an electric response and are isotropic on the plane of the interface, the ABCD matrix of a single admittance layer can be written as

$$\boldsymbol{Y}^i_{s,n} = \begin{pmatrix} 1 & 0 \\ 1/jX^i_{s,n} & 1 \end{pmatrix}. \tag{4}$$

Finally, from the ABCD matrix (2), by using (3) and (4), the ABCD matrix of the single cell can be related to its transmission and reflection coefficients through the relations [61]

$$\begin{aligned} S^n_{2,1}\left(Y^i_{s,n}, d\right) &= \frac{2}{A_n + B_n/\eta_0 + \eta_0 C_n + D_n} \\ S^n_{1,1}\left(Y^i_{s,n}, d\right) &= \frac{A_n + B_n/\eta_0 - \eta_0 C_n - D_n}{A_n + B_n/\eta_0 + \eta_0 C_n + D_n}. \end{aligned} \tag{5}$$

The transmission (reflection) coefficient values, in both amplitude and phase, of the single HMS unit-cell are thus controlled by the dielectric material properties and the surface impedances of the ideal impedance sheets. It is worth noting that (5) uses the canonical scattering parameters transformation, assuming a moderate value of φ. Conversely, the generalized scattering parameters [63] should be eventually used to properly satisfy the local power conservation requirement ensuring the matching of the different wave impedances at the cell sides [60].

Through the above formalism, we can design the $2N-1$ discrete cells that guarantee the desired phase-insertion profile resulting from (1). Indeed, once the dielectric characteristics and the number of layers I are fixed, (5) can be used to find the proper combinations of the surface impedance values $Z^1_{s,n}$, $Z^i_{s,n}, \ldots, Z^I_{s,n}$ satisfying the following conditions:

$$arg\left(S^n_{2,1}\right) = \Phi(\varphi_n), \quad \left|S^n_{2,1}\right| = 1. \tag{6}$$

From a theoretical point of view, the availability of an analytical model allows the synthesis of the surface impedance values of the nth unit-cell composing the HMS. However, the complexity of the analytical formulation and the underdetermined nature of the resulting algebraic system make this approach not feasible. Therefore, as described in [62], for the design of the nth unit-cell satisfying (6), the cascade matrix model is used to numerically compute a database of transmission coefficient values of a single stacked HMS unit-cell for different combinations of $Z^1_{s,n}$, $Z^i_{s,n}, \ldots, Z^I_{s,n}$.Finally, among all the solutions returned, only the ones satisfying (6) are considered.

III. Numerical Examples of Beamforming HMS Coatings

To prove the validity and the potentiality of this approach, here, we apply the proposed design workflow to several study cases. In particular, the synthesis of different cylindrical HMSs aiming at tuning the EM radiation characteristics of a coated antenna is reported. The formalism previously presented is discussed when considering ideal lossless impedance transition sheets (i.e., $Z^i_{s,n} = jX^i_{s,n}$ is assumed), and the numerical results for the different configurations are reported.

A. Four-Sector Antenna

As a first example, we detail the synthesis of a cylindrical HMS able to focus the field radiated by a linear antenna source toward four symmetric directions. The HMS is divided into four focusing sections characterized by the same phase-gradient profile, as shown in Fig. 3. Thus, the spatial periodicity of $\Phi(\varphi)$ is $\pi/2$. As a reference, the feeding antenna is designed to work at the central frequency $f_0 = 2.5$ GHz (albeit the design can be easily scaled at other frequencies), while the HMS radius is $a_c = \lambda_0/2$. This value is chosen as a trade-off between the space occupancy of the coating and the minimum distance allowing the HMS to work properly. Further reducing the coating aspect ratio would put the HMS in the very near-field of the antenna, massively compromising the HMS response. Indeed, when placing the HMS in the reactive region of the antenna (i.e., before the Fresnel region [45]), colocation of the electric and magnetic dipole moments is quite difficult. Moreover, as can be inferred from Fig. 2, extremely small unit-cells would be required to sample uniformly the coating metasurface and guarantee a smooth discretization of $\Phi(\varphi)$ due to the reduced HMS area.

For the implementation of the metasurface, each section is also discretized in $2N-1 = 15$ unit-cells providing the desired phase-insertion, i.e., ensuring the required phase shift for each of the nth cells. The latter is evaluated by introducing the

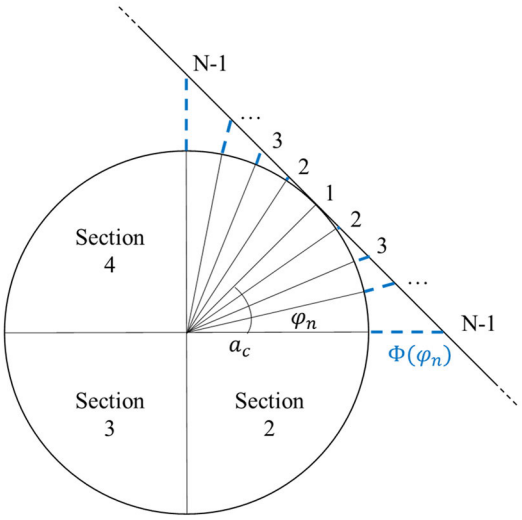

Fig. 3. Two-dimensional geometrical sketch of the division in sections and sectors of the cylindrical HMS returning a four-beam symmetrical radiation pattern. Each section is discretized through N unit-cells introducing a phase shift $\Phi(\varphi_n)$. φ_n represents the angular position of the nth unit-cell with reference to the center of the section.

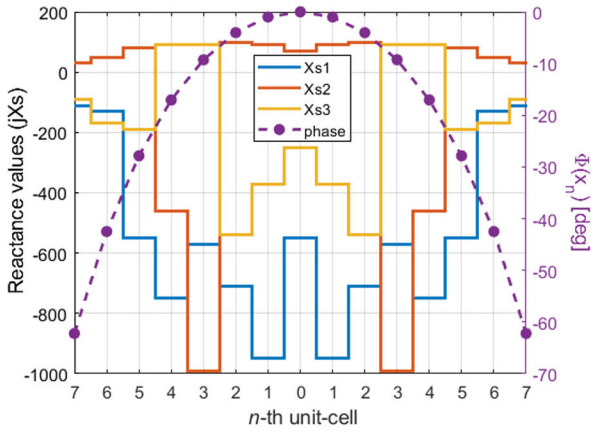

Fig. 4. Reactance values (imaginary parts) of the first (X_s^1), second (X_s^2), and third (X_s^3) impedance layers of the metasurface discretized in 15 unit-cells for the four-beam HMS case (continuous lines). Phase-insertion returned by the 15 unit-cells. The X_s measurement unit is Ω/sq (dashed line).

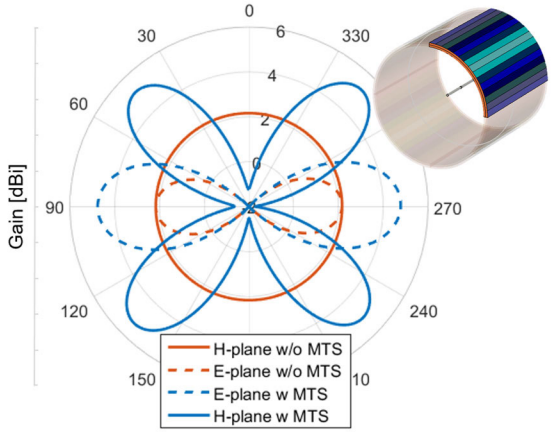

Fig. 5. Gain polar plots of the four-beam HMS-coated antenna and of the bare dipole (blue and red lines, respectively) on the H-plane (continuous line) and E-plane (dashed line). In the inset, the sketch of the coated antenna highlighting a single HMS sector is reported. The different colors of the unit-cells pictorially represent the metasurface phase gradient in the azimuthal direction.

referenced f_0 and a_c values in (1), leading to $\varphi_n = n\varphi = n6°$ and, thus, with the discretized phase-insertion function $\Phi(\varphi_n)$ introducing a phase coverage $\Delta\Phi(\varphi_n) = |\Phi(\varphi_8) - \Phi(\varphi_1)| = 62°$, as resumed in Fig. 4.

Finally, exploiting the matrix representation and formalism reported in (5), it is found that this phase range is easily covered by unit-cells consisting of two dielectric substrates ($t = \lambda_0/60$, $\varepsilon_r = 10$) sandwiched between three purely reactive transition sheets. In particular, the combinations of surface reactances $X_{s,n}^1$, $X_{s,n}^2$, $X_{s,n}^3$ satisfying the first equation in (6) with $|S_{2,1}^n| \geq 0.9$ are in the range $[-990, +100]$ Ω/sq. The different values of the surface impedances used to implement the 15 unit-cells and the corresponding phase-insertions are reported in Fig. 4.

The analytically designed unit-cells are implemented in a full-wave EM simulation tool as subwavelength constituents of the cylindrical HMS coating. Since the HMS aims at introducing a phase-gradient only on the H-plane, the individual HMS unit-cells are invariant along the E-plane, as can be observed in the sketch reported in the inset of Fig. 5. In other terms, a vertically homogeneous distribution of square cells is assumed along the axis of the cylindrical coating.

Finally, in Fig. 5, the 2-D gain behavior of the designed phase-gradient HMS is reported and compared to the uncoated antenna scenario. The gain polar plots are evaluated on both H- and E-planes, with the latter considered along the plane of maximum directivity (i.e., for $\varphi = 45°$). Thanks to the focusing effect coming from the four metasurface sections, four main radiating beams are observed, and the original constant gain value of the uncoated antenna increases to 4.98 dBi. At the same time, due to the absence of a phase-gradient along the z-axis, the original *inverted-8* shape of the radiation pattern is unaltered on the E-plane, though with a different absolute value due to the power-conservation principle. Still, the half-power beamwidth (HPBW) on the E-plane is the same in both cases.

It is worth noting that by reconfiguring the sheet reactance values of the unit-cells, the beams rotate and dynamic coverage on the horizontal plane is enabled. Arguably, similar behavior can be assessed either using four independent radiating elements (see as an example [64]) or by employing electronically steerable parasitic array radiator antennas (ESPAR) [65]. Still, compared to the former solution, here, the rotation of the beams is obtained through a single radiator coated by the proposed HMS. While in the latter case, the use of parasitic radiators increasing the antenna space occupancy and loaded with high-value complex reactive load controls can be required. Moreover, the limited number of passive elements that can be used can further limit the scanning spatial resolution.

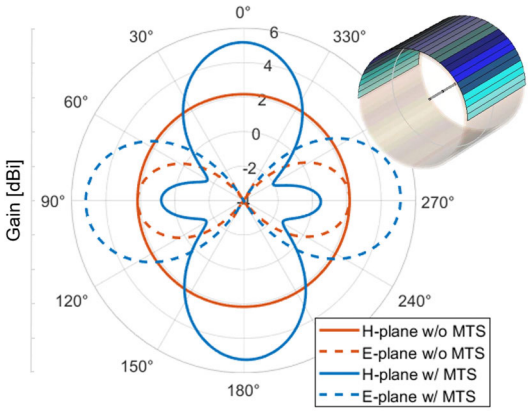

Fig. 6. Gain polar plots of the two-beam HMS-coated antenna and of the bare dipole (blue and red lines, respectively) on the H-plane (continuous line) and E-plane (dashed line). In the inset, the sketch of the coated antenna highlighting a single HMS sector is reported. The different colors of the unit-cells pictorially represent the metasurface phase gradient in the azimuthal direction.

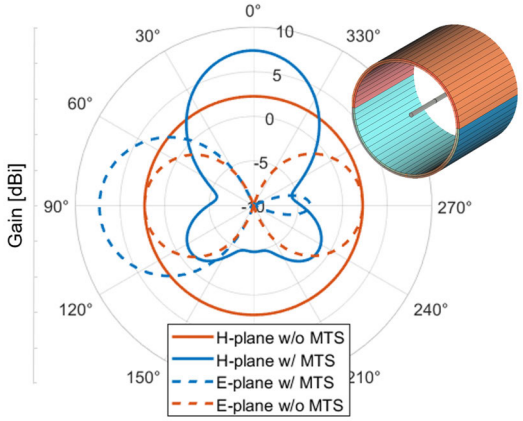

Fig. 7. Gain polar plots of the single-beam HMS-coated antenna and of the bare dipole (blue and red lines, respectively) on the H-plane (continuous line) and E-plane (dashed line). In the inset, the sketch of the coated antenna highlighting the reflective and transmitting sectors are reported (blue and orange semi-cylindrical surfaces, respectively).

B. Two-Sector Antenna

To demonstrate the versatility of our approach in achieving beamforming functionality, we also report another design case considering a dual-beam HMS-coated linear antenna. The design procedure follows the one described in the previous case. However, here, the spatial periodicity of the phase-insertion function $\Phi(\varphi)$ is set to π. Namely, the cylindrical metasurface is divided into two equal surfaces introducing the same phase-gradient distribution, as pictorially represented in the inset of Fig. 6.

To keep the same unit-cell dimension of the previous scenario, guaranteeing proper homogenization of the metasurface, the HMS is discretized in $2N - 1 = 30$ unit-cells. The phase-insertion is still evaluated through (1), returning a discretized phase-insertion function $\Phi(\varphi_n)$, requiring a phase coverage in the range $\Delta\Phi(\varphi_n) = |\Phi(\varphi_{15}) - \Phi(\varphi_1)| = -740°$. Thus, the unit-cell configuration should be able to cover a full 2π phase range. Namely, the same three-layered structure previously considered is used, and the $X^1_{s,n}$, $X^2_{s,n}$, $X^3_{s,n}$ are synthetized selecting, from the database of combinations compliant with the first equation in (6), the ones still providing $|S^n_{2,1}| \geq 0.9$. Here, the surface reactance values composing the three layers of the metasurface and returning the desired phase coverage are in the range $[-940, +90]$ Ω/sq.

The full-wave numerical results of the designed structure are reported in Fig. 6. The polar plot gain shows two main lobes pointing in opposite directions on the H-plane, with a maximum gain of 5.17 dBi. As in the previous example, the shape of the radiation pattern remains almost unaltered on the E-plane with beams characterized by the same HPBW.

C. Single-Sector Scanning Antenna

Though in the previous examples, we focused on devices leading to multibeam configurations, the coating metasurface can be also designed to generate a single radiating beam that can be used for scanning on the H-plane.

A sketch of this antenna is depicted in the inset of Fig. 7. Importantly, compared to the previous cases presented, here a reflective metasurface is introduced. Namely, the cylindrical coating is divided into two symmetric sectors, as in the previous example, but one sector is characterized by perfectly reflective unit-cells (the blue sector in Fig. 7), while the other one is designed following the procedure used so far for the design of an HMS (the orange sector in Fig. 7). The latter section relies on the use of a full-transmitting semi-cylindrical HMS, while the former is constituted by nth reflective unit-cells with the same values of X^1_s, X^2_s, X^3_s. In this case, the surface reactances are found exploiting the reflection coefficient formula in (5) and imposing the condition

$$arg\left(S^n_{1,1}\right) = \Phi' = 2(\pi - k_0 a_c), \quad \left|S^n_{1,1}\right| \cong 1. \tag{7}$$

Equation (7) ensures constructive interference between the field reflected by the reflecting sector and the one transmitted through the HMS sector. When considering $a_c = \lambda_0/2$, (7) returns $arg(S^n_{1,1}) = 0$ and the surface reactance values satisfying this condition are $X^1_s = -72$, $X^2_s = 72$, and $X^3_s = -6$ Ω/sq.

It is worth noticing that the condition $arg(S^n_{1,1}) = 0$ differs from the one of a conventional reflector made of a perfect electric conductor (PEC) where the distance between the antenna and the reflector should be $d = \lambda_0/4$ [45] (which in (7) leads to the condition $arg(S^n_{1,1}) = \pi$). Importantly, (7) is not restricted to a specific value of a_c but allows designing a cylindrical reflective panel for any distance value, increasing the degree of freedom compared to conventional metallic reflective panels. It is also important to stress that the cells designed for the back-reflective sector are not Huygens cells as the ones used for the front transmissive sector.

Finally, in Fig. 7, the gain performance of the antenna coated by the cylindrical metasurface is reported. As can be appreciated from the polar plot, a directive beam appears on the H-plane with a maximum gain of 7.33 dBi. Remarkably, by making the metasurface unit-cell reconfigurable, it can be envisioned a system where the radiation characteristics of

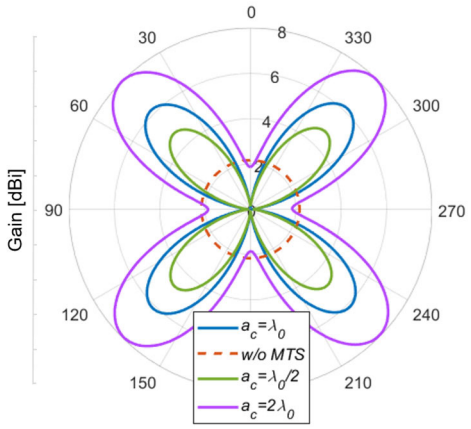

Fig. 8. Gain polar plots evaluated on the H-plane for different four-beam HMS-coated antennas when the HMS radius is $a_c = \lambda_0/2, \lambda_0, 2\lambda_0$ (continuous green, blue, and purple lines, respectively). Bare antenna (red dashed line).

the antenna can be switched from the ones of an omnidirectional radiator to the ones of a directive transmitting/receiving antenna system able to scan the horizontal plane. In the next section, a reconfigurable system is designed to address this vision.

To conclude this section, we report some insightful remarks on the relation between the directivity of the beamformed radiation pattern and the HMS aspect ratio. In Fig. 8, the results for three different configurations of the four-beam HMS-coated linear antenna are reported. The metasurface coatings differ in the value of the parameter a_c, i.e., for the dimension of the HMS radius. In particular, the cases for $a_c = \lambda_0/2, \lambda_0, 2\lambda_0$ are reported. The coating layers have been designed following the conventional procedure and evaluating (1) considering the three different values of a_c. Moreover, the same unit-cell dimension has been considered for the different configurations. Thus, due to the increase of the HMS area when increasing its radius, each focusing sector has been implemented with $2N-1 = 15, 30$, and 60 cells, respectively.

From Fig. 8, a massive increase in the maximum directivity value can be observed. Arguably, the increase in the directivity comes from the extended equivalent radiating area of the coating metasurface, demonstrating that a trade-off between the maximum gain and the HMS aspect ratio is always needed. It is worth mentioning that when reducing a_c to less than $\lambda_0/4$, the directivity massively reduced due to the weakening of the effectiveness of the approach proposed. Indeed, the phase-gradient introduced by the HMS should be obtained in a reduced space, possibly introducing a stronger phase discontinuity among the cells and lowering performance. Moreover, the metasurface would be in the very near-field of the antenna compromising the response of the Huygens cells and the proper co-location of the electric and magnetic dipoles.

IV. Realistic Configuration of a Dynamic Beamforming Linear Antenna

We have shown that, by properly tuning the phase-insertion profile of a cylindrical HMS along the azimuthal plane, the radiation pattern of a linear antenna can be shaped in different ways. Since the $\Phi(\varphi)$ profile is controlled by modifying the responses of the individual unit-cells, i.e., it can be tuned by controlling the surface impedance values of the cells, here, we explore the possibility to add reconfigurability to a preselected beamforming system. In particular, we focus our attention on the realistic configuration of the multibeam device reported in Fig. 5, with the aim of implementing an antenna radiation pattern that can be dynamically switched between different configurations. For this purpose, the design of realistic and feasible unit-cells is considered, as well as the use of varactor diodes to tune the phase-insertion provided by the HMS cells.

One of the key aspects when dealing with metasurfaces equipped with varactor diodes is the minimization of the number of electronic elements to reduce the losses and the overall cost of the structure. At the scope, hereinafter, we consider unit-cells implemented through two-impedance sheets sandwiching a dielectric spacer, where the top layer is loaded with a varactor to tune the phase-insertion introduced by the cell. In other terms, the cell consists of a top dynamic layer characterized by a variable X_s^1, modified thanks to the varactor loading, and a bottom static layer with a fixed value of the X_s^2. This structure ensures the minimization of the number of electronic elements required to modulate the $\Phi(\varphi)$. Moreover, to further minimize the number of varactors, the HMS is implemented through a coarse discretization of the unit-cells. Namely, $2N-1 = 5$ cells are used for one metasurface sector (i.e., for each $\Phi(\varphi)$ period), leading to square unit-cells having a length $l = \lambda_0/5$. It is worth mentioning that, though the discretization is rather course, the effectiveness of this strategy has been recently demonstrated in [68].

As a first step of the design, the characteristics of the dielectric substrate are defined. In particular, the commercial dielectric Rogers RO3006 ($\varepsilon_r = 6.15$, $tan\delta = 0.002$) is selected for its flexibility toward bending, which makes it particularly suited for curved surfaces. To determine the value of the substrate thickness t, the $arg(S_{2,1}^n)$ coming from (5) for $\varepsilon_r = 6.15$ and $f_0 = 2.5$ GHz is evaluated when varying the parameters t, X_s^1 and X_s^2. Since to properly design a two-layer HMS unit-cell both inductive ($X_s \geq 0$) and capacitive ($X_s \leq 0$) sheets are required, the X_s^1 and X_s^2 are considered in the realistic ranges of $[-1000, 0]$ and $[0, +300]$ Ω/sq, respectively, while t varies according to the values available from the RO3006 datasheet.

In Fig. 9, the results filtered out for $|S_{2,1}^n| \geq 0.9$ are reported. For $t \geq 1.5$ mm, a smooth phase variation within the range required for the four-beam HMS scenario (i.e., $\Delta\Phi(\varphi_n) = 62°$) is guaranteed. Thus, $t = 1.5$ mm is selected as the thickness for the substrate. We remark that, although larger values of t guarantee even smoother coverage, a further increase in the dielectric thickness would compromise the flexibility of the substrate.

Once the characteristics of the substrate have been defined, the optimum value for the static surface impedance X_s^2 of the bottom layer is fixed. For this purpose, (5) is once again evaluated but for $t = 1.5$ mm. The behavior of $arg(S_{2,1}^n)$ for fixed values of the X_s^2 and varying X_s^1 is reported in Fig. 10. As can be seen, the phase coverage massively depends on the

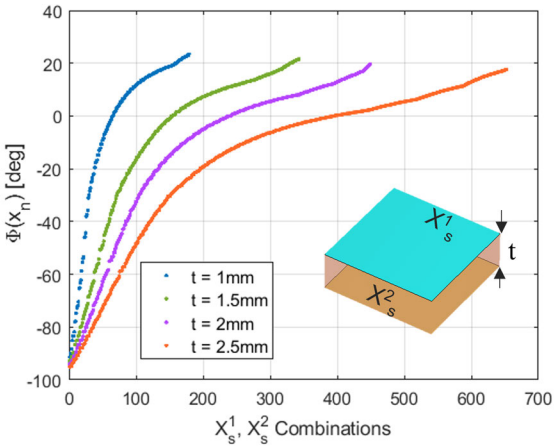

Fig. 9. Phase coverage $\Phi(\varphi_n)$ returned by (5) for a unit-cell made of a dielectric substrate with $\varepsilon_r = 6.15$ sandwiched between two impedance layers (in the inset) when considering different combinations of the surface reactances X_s^1 and X_s^2, and when varying the thickness t of the spacer. The ranges considered for X_s^1 and X_s^2 are $[-1000, 0]$ and $[0, +300]$ Ω/sq, respectively.

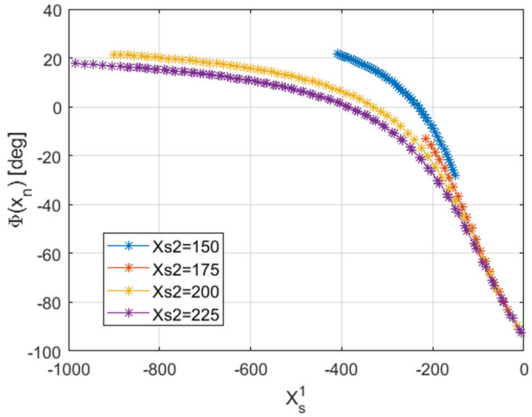

Fig. 10. Phase coverage $\Phi(\varphi_n)$ returned by (5) for a two-layer unit-cell separated by a dielectric substrate with $\varepsilon_r = 6.15$ and $t = 1.5$ mm, when X_s^2 is fixed and X_s^1 varies. The X_s measurement unit is Ω/sq.

static value of X_s^2. In particular, the widest phase coverage is achieved for $X_s^2 = 225$ Ω/sq. This value guarantees, in principle, the full coverage of the phase-insertion profile in Fig. 4 when varying X_s^1 within realistic values. We stress that further increasing the value of X_s^2 would make the synthesis of a realistic inductive layer more difficult. Arguably, a high value of the X_s^2 requires the synthesis of an impedance layer characterized by an extremely high inductive response, which can be quite cumbersome to achieve when considering feasible layouts. Hence, the value of the X_s^2 is fixed to 225 Ω/sq.

To practically implement the inductive layer returning an $X_s^2 = 225$ Ω/sq, a simple and feasible layout consisting of a single metallic strip etched on the bottom face of the dielectric spacer is used, as shown in the inset of Fig. 11. As known [66], [67], this design returns a unit-cell exhibiting an inductive response when excited by a TE polarized wave ($E_z \neq 0$, $E_x = E_y = 0$). Exploiting the analytical formulas in [66] and considering the presence of the dielectric substrate and the unit-cell dimension, it is found that $X_s^2 = 225$ Ω/sq is achieved when the width of the metallic strip is $w_L = \lambda_0/160$.

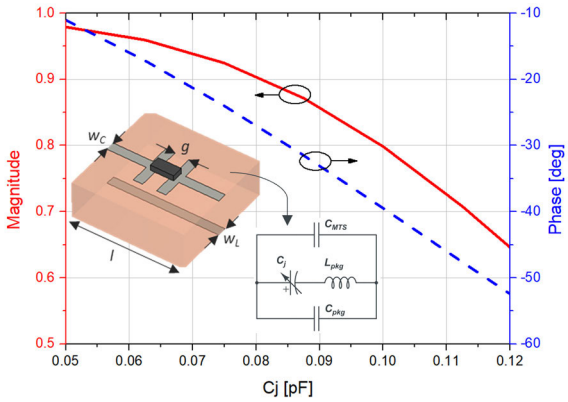

Fig. 11. Transmission coefficient values (S_{21}) in amplitude and phase of the reconfigurable HMS unit-cell when varying the junction capacitance (C_j) of the varactor. In the insets, a sketch of the varactor-loaded unit-cell and the equivalent circuit schematic of the top layer, are reported.

Conversely, for the design of the capacitive layer, a metallic strip with a gap in the middle is considered. The gap is then loaded with a varactor to tune the surface impedance value, as depicted in the inset of Fig. 11. This configuration can be modeled as the parallel combination between the load capacitance and the equivalent capacitance introduced by the patterned surface C_{mts}. Namely, in the inset of Fig. 11, the circuit schematic of the unit-cell top layer is exemplified (neglecting the internal diode resistance R_s for convenience). Here, C_j represents the junction capacitance of the varactor, while C_{pkg} and L_{pkg} represent the parasitic reactive effects due to the packaging. The required junction capacitance $C_{j,n}$ to get the needed value of the nth unit-cell $X_{s,n}^1$ can be thus evaluated as

$$C_{j,n} = \frac{C_{mts} + C_{pkg} - C_n}{1 + \left(C_n - C_{mts} - C_{pkg}\right)\omega^2 L_{pkg}} \tag{8}$$

where $C_n = -1/\omega X_{s,n}^1$. By defining the desired range of variation for X_s^1 and by fixing the maximum and minimum values of the $C_{j,n}$, the final dimensions of the capacitive strip can be derived. In particular, from Fig. 10, it can be inferred that to cover the required phase-insertion $\Delta\Phi(\varphi_n) = 62°$, $X_{s,n}^1$ should vary between $-1000 \leq X_{s,n}^1 \leq -100$. For the variation range of $C_{j,n}$, realistic values for the commercial varactor diode MGV125-08 from MACOM (with $L_{pkg} = 0.4$ nH, $C_{pkg} = 80$ fF) are considered. Namely, the varactor capacitance varies from about 0.6 to 0.05 pF when its reverse voltage changes from 2 to 20 V.

Hence, the final dimensions of the capacitive top strip are $w_C = \lambda_0/92$ and $g = \lambda_0/40$, and the transmission coefficient behavior for the unit-cell when excited by *Floquet* modes under TE illumination is reported in Fig. 11, in both amplitude and phase. As can be appreciated, when varying C_j within (0.05–0.13 pF) the desired phase range is covered. However, due to the realistic configuration of the layout, the amplitude of the transmission coefficient degrades more significantly compared to the ideal setup, especially for large phase shift values. Anyway, we remark here that only the external unit-cells of a single metasurface sector require such

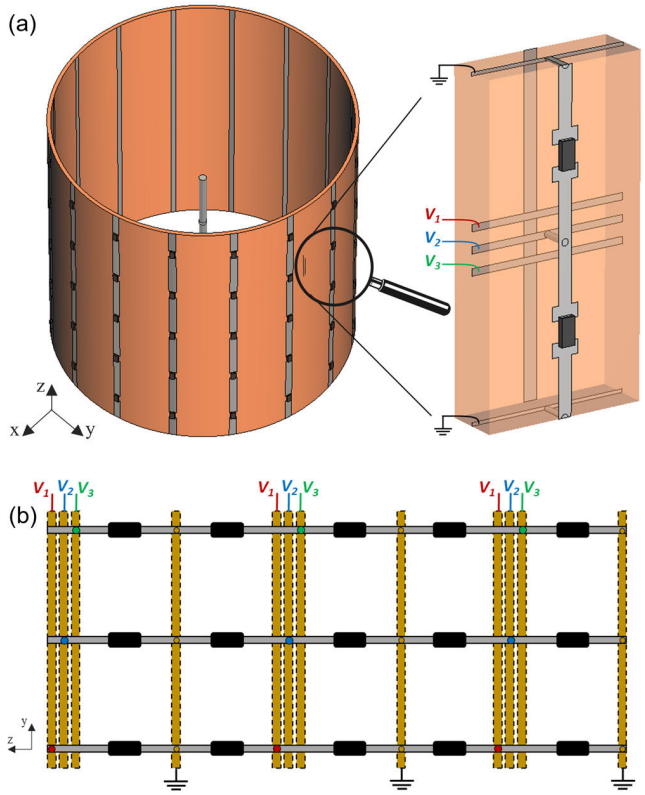

Fig. 12. (a) Sketch of the realistic HMS coating surrounding the dipole antenna introducing a phase-gradient on the *xoy*-plane. The HMS consists of a dual-layer metasurface made of inductive metallic strips and capacitive strips loaded with varactor diodes. In the inset, the zoom of two vertically consecutive unit-cells showing the biasing network layout is reported. (b) Pictorial schematic of one half of the metasurface sector in the planar configuration when considering the top reconfigurable layer and the biasing network embedded in the cell substrate. The black boxes represent the varactors; the gray lines are the top capacitive strips; the yellow dashed lines represent the cross-polarized biasing lines. (Dimensions of the biasing lines are not in scale.)

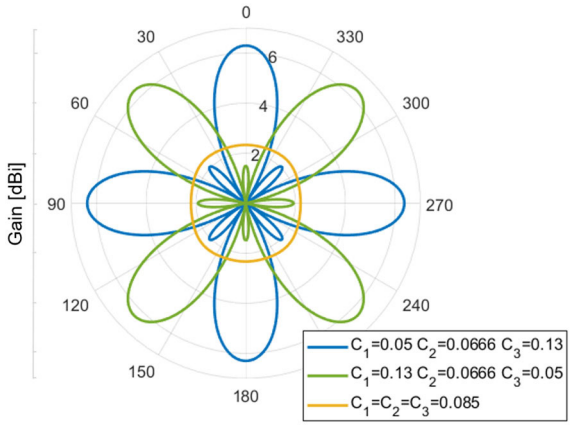

Fig. 13. Gain polar plots evaluated on the H-plane of the antenna for different combinations of the varactors' junction capacitance $C_{j,n}$. The values of the junction capacitances are expressed in (pF).

a large phase shift value. Thus, acceptable overall performance is expected.

A sketch of the final cylindrical HMS coating surrounding the dipole antenna is reported in Fig. 12(a). As can be appreciated, all cells are characterized by the same physical layout since the different phase-insertion values are achieved by properly tuning the varactors. In the zoom showing two consecutive unit-cells distributed along the z-axis, the biasing lines of the diodes are also reported, while in Fig. 12(b), the schematic of the one-half metasurface sector in planar configuration is illustrated. In the latter, just the top reconfigurable layer and the biasing network are reported for convenience. It can be observed that the network is embedded within the dielectric substrate and consists of two grounded horizontal strips (used as voltage reference), and another set of three strips connected to the top capacitive layer through a metallic via for setting the polarization voltages. The top strips are bridged to the V_n (with $n = 1, 2, 3$) through a single via that is alternatively connected to the polarizing strips depending on the desired phase insertion introduced by the cell [see the red/blue/green dots in Fig. 12(b)]. It is worth noticing that the ultrathin biasing lines are cross-polarized with reference to the antenna. Hence, the coupling with the field radiated by the source and the inductive/capacitive strips is almost negligible.

In Fig. 13, the numerical results of the coated antenna evaluated through full-wave simulations are reported. The gain polar plot shows that by adjusting the biasing voltages for setting the $C_{j,n}$ in the range (0.05–0.13 pF), four main radiating beams appear, with a maximum gain of 6.34 dBi. Remarkably, when setting the junction capacitances of all the varactors to 0.085 pF, the original omnidirectional pattern of the antenna is restored, emphasizing the reconfiguration capability of the system. Furthermore, the possibility to control the phase-insertion of the single cells allows to dynamically rotate the radiation pattern on the antenna H-plane, further expanding the scanning and steering capability of the device. It is worth noticing that in Fig. 13 just two steering configurations are reported (see the blue and green curves). However, by properly tuning the varactors, other intermediate point angles can be obtained that are, however, here omitted for improving the clarity of the figure. At the same time, on the E-plane, the shape of the radiation pattern is unaltered compared to the bare antenna scenario, as can be appreciated from the 3-D radiation pattern in Fig. 14.

Albeit the presence of the HMS coating around the linear antenna, the matching performances are quite good, as shown in Fig. 15, where the reflection coefficient magnitude at the antenna input port is reported and compared with the one of the bare dipole. A slight shift of the central operation frequency and a reduction of the bandwidth can be observed, although at f_0 still good matching is achieved. The performance deterioration is mostly due to the non-ideal transmission performance of the metasurface unit-cells that partially reflect the field radiated by the source, inducing secondary currents that modify the original behavior.

Finally, in Fig. 16, the performance of the realistic HMS configuration is compared to the ideal setup discussed in Section III. As expected, a deterioration of the gain response of the realistic design can be noticed, with an almost 1 dB

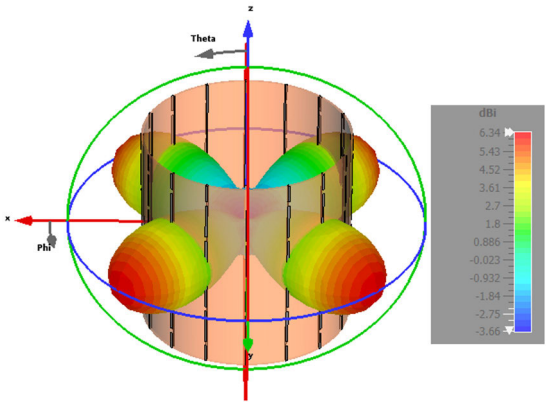

Fig. 14. Three-dimensional gain radiation pattern of the antenna for the varactors' junction capacitances combination ensuring the four-beam configuration.

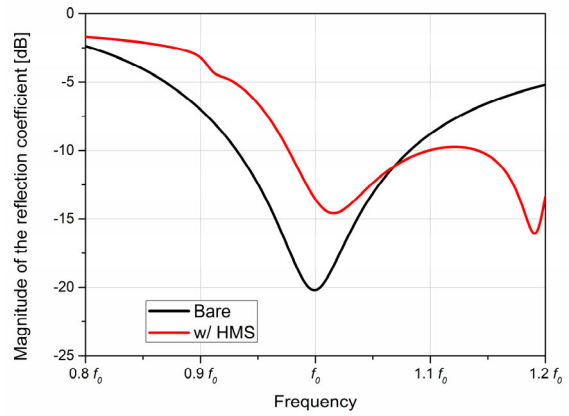

Fig. 15. Magnitude of the reflection coefficient at the antenna input port for the scenarios w/o (black line) and w/ (red line) the HMS coating once the varactors are set to ensure the four-beam configuration.

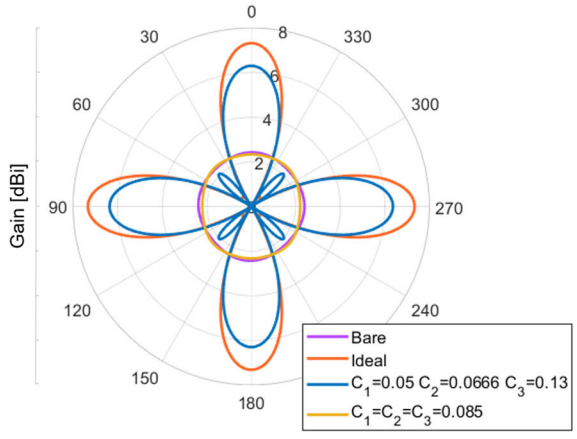

Fig. 16. Gain polar plots evaluated on the H-plane of the antenna when the junction capacitances of the varactors are set to achieve a four-beam pattern (blue line) or an omnidirectional pattern (orange line). For comparison, the equivalent configuration when considering the ideal HMS unit-cell is reported (red line), as well as the original dipole antenna pattern (purple line).

reduction of the maximum gain. However, this reduction was expected and reasonable considering the simplicity of the ideal layout, the inclusion of the biasing network, and the presence of losses coming from both the dielectric and the varactors. Moreover, we underline that, in the above full-wave simulations, the internal resistance of the varactors was included ($R_s = 2.65\ \Omega$ from the varactor datasheet), although not considered in the first instance in the circuit schematic in Fig. 11. Thanks to the reduced number of varactors, the low value of R_s, and the non-resonant behavior of the impedance sheets, the radiation efficiency of the antenna is quite high and equal to $e_{rad} = 0.9$, confirming the benefit of the proposed design strategy.

V. Conclusion

In this article, we have shown that beamforming functionality can be introduced in linear antenna systems by means of phase-gradient HMS surrounding a single simple radiator like a dipole. In particular, we have shown that the original omnidirectional radiation pattern of the dipole antenna can be turned into multiple- or single-beam shapes through a judicious design of the HMS and, thus, by properly engineering its phase-insertion profile.

At the scope, a complete design procedure has been developed, highlighting the working principle of the structure and deriving closed-form formulas for identifying the required phase-insertion profile. In addition, a semi-analytical procedure for designing the HMS characterized by the desired phase-gradient profile has been reported, exploiting a conventional network approach. The effectiveness of the proposed design workflow has been assessed by using it for the synthesis of cylindrical HMSs enabling different beamforming effects. Finally, a realistic configuration of a phase-gradient HMS coating for dynamic beamforming functionalities has been presented. The reconfigurability of the system was achieved by loading the HMS with varactor diodes able to tune the phase-insertion exhibited by the individual unit-cells. For the unit-cell design, particular emphasis has been put on the minimization of the losses coming from the use of commercial electronic elements. This approach allowed for achieving good efficiency and reasonable overall performance, as confirmed by the final numerical simulation results.

The possibility to dynamically shape the radiation pattern of such a simple antenna could find interesting applications in both outdoor and indoor wireless communications. Indeed, the device could be used in smart radio BTS and/or smart repeaters for dynamically rerouting the signal toward specific directions or multiple users, according to the operative and environmental conditions. Moreover, these findings confirm the effectiveness of conformal cylindrical metasurfaces as a promising solution for implementing "intelligent" antennas capable of reconfiguring their frequency, scattering, and radiation responses.

References

[1] L. Bariah et al., "A prospective look: Key enabling technologies, applications and open research topics in 6G networks," *IEEE Access*, vol. 8, pp. 174792–174820, 2020.

[2] J. Zhang, E. Björnson, M. Matthaiou, D. W. K. Ng, H. Yang, and D. J. Love, "Prospective multiple antenna technologies for beyond 5G," *IEEE J. Sel. Areas Commun.*, vol. 38, no. 8, pp. 1637–1660, Aug. 2020.

[3] A. Ijaz et al., "Enabling massive IoT in 5G and beyond systems: PHY radio frame design considerations," *IEEE Access*, vol. 4, pp. 3322–3339, 2016.

[4] H. Frank, C. Colman-Meixner, K. D. R. Assis, S. Yan, and D. Simeonidou, "Techno-economic analysis of 5G non-public network architectures," *IEEE Access*, vol. 10, pp. 70204–70218, 2022.

[5] T. S. Rappaport et al., "Millimeter wave mobile communications for 5G cellular: It will work!" *IEEE Access*, vol. 1, pp. 335–349, 2013.

[6] K. Aldubaikhy, W. Wu, N. Zhang, N. Cheng, and X. Shen, "mmWave IEEE 802.11ay for 5G fixed wireless access," *IEEE Wireless Commun.*, vol. 27, no. 2, pp. 88–95, Apr. 2020.

[7] I. K. Jain, R. Kumar, and S. S. Panwar, "The impact of mobile blockers on millimeter wave cellular systems," *IEEE J. Sel. Areas Commun.*, vol. 37, no. 4, pp. 854–868, Apr. 2019.

[8] J. Du, D. Chizhik, R. Feick, M. Rodríguez, G. Castro, and R. A. Valenzuela, "Suburban fixed wireless access channel measurements and models at 28 GHz for 90% outdoor coverage," *IEEE Trans. Antennas Propag.*, vol. 68, no. 1, pp. 411–420, Jan. 2020.

[9] L. Chiaraviglio et al., "Planning 5G networks under EMF constraints: State of the art and vision," *IEEE Access*, vol. 6, pp. 51021–51037, 2018.

[10] L. Chiaraviglio, C. Di Paolo, and N. Blefari-Melazzi, "5G network planning under service and EMF constraints: Formulation and solutions," *IEEE Trans. Mobile Comput.*, vol. 21, no. 9, pp. 3053–3070, Sep. 2022.

[11] M. D. Renzo et al., "Smart radio environments empowered by reconfigurable AI meta-surfaces: An idea whose time has come," *EURASIP J. Wireless Commun. Netw.*, vol. 2019, no. 1, pp. 1–20, Dec. 2019.

[12] M. Di Renzo et al., "Smart radio environments empowered by reconfigurable intelligent surfaces: How it works, state of research, and the road ahead," *IEEE J. Sel. Areas Commun.*, vol. 38, no. 11, pp. 2450–2525, Nov. 2020.

[13] F. Yang, D. Erricolo, and A. Massa, "Special issue on smart electromagnetic environment," *IEEE Trans. Antennas Propag.*, vol. 69, no. 3, p. 1838, Mar. 2021.

[14] A. Massa et al., "Designing smart electromagnetic environments for next-generation wireless communications," *Telecom*, vol. 2, no. 2, pp. 213–221, May 2021.

[15] G. Gradoni et al., "Smart radio environments," 2021, *arXiv:2111.08676*.

[16] M. Barbuto et al., "Metasurfaces 3.0: A new paradigm for enabling smart electromagnetic environments," *IEEE Trans. Antennas Propag.*, vol. 70, no. 10, pp. 8883–8897, Oct. 2022.

[17] E. Martini and S. Maci, "Theory, analysis, and design of metasurfaces for smart radio environments," *Proc. IEEE*, vol. 110, no. 9, pp. 1227–1243, Sep. 2022.

[18] A. Díaz-Rubio, S. Kosulnikov, and S. A. Tretyakov, "On the integration of reconfigurable intelligent surfaces in real-world environments: A convenient approach for estimation reflection and transmission," *IEEE Antennas Propag. Mag.*, vol. 64, no. 4, pp. 85–95, Aug. 2022.

[19] R. Flamini et al., "Toward a heterogeneous smart electromagnetic environment for millimeter-wave communications: An industrial viewpoint," *IEEE Trans. Antennas Propag.*, vol. 70, no. 10, pp. 8898–8910, Oct. 2022.

[20] G. Oliveri, P. Rocca, M. Salucci, and A. Massa, "Holographic smart EM skins for advanced beam power shaping in next generation wireless environments," *IEEE J. Multiscale Multiphys. Comput. Techn.*, vol. 6, pp. 171–182, 2021.

[21] G. Oliveri, F. Zardi, P. Rocca, M. Salucci, and A. Massa, "Building a smart EM environment–AI-enhanced aperiodic micro-scale design of passive EM skins," *IEEE Trans. Antennas Propag.*, vol. 70, no. 10, pp. 8757–8770, Oct. 2022, doi: 10.1109/TAP.2022.3151354.

[22] E. Basar, M. Di Renzo, J. D. Rosny, M. Debbah, M.-S. Alouini, and R. Zhang, "Wireless communications through reconfigurable intelligent surfaces," *IEEE Access*, vol. 7, pp. 116753–116773, 2019.

[23] M. Di Renzo et al., "Reconfigurable intelligent surfaces vs. relaying: Differences, similarities, and performance comparison," *IEEE Open J. Commun. Soc.*, vol. 1, pp. 798–807, 2020.

[24] M. A. ElMossallamy, H. Zhang, L. Song, K. G. Seddik, Z. Han, and G. Y. Li, "Reconfigurable intelligent surfaces for wireless communications: Principles, challenges, and opportunities," *IEEE Trans. Cognit. Commun. Netw.*, vol. 6, no. 3, pp. 990–1002, Sep. 2020.

[25] V. Degli-Esposti, E. M. Vitucci, M. D. Renzo, and S. A. Tretyakov, "Reradiation and scattering from a reconfigurable intelligent surface: A general macroscopic model," *IEEE Trans. Antennas Propag.*, vol. 70, no. 10, pp. 8691–8706, Oct. 2022, doi: 10.1109/TAP.2022.3149660.

[26] M. Di Renzo and S. Tretyakov, "Reconfigurable intelligent surfaces," *Proc. IEEE*, vol. 110, no. 9, pp. 1159–1163, Sep. 2022.

[27] R. Liu, Q. Wu, M. Di Renzo, and Y. Yuan, "A path to smart radio environments: An industrial viewpoint on reconfigurable intelligent surfaces," *IEEE Wireless Commun.*, vol. 29, no. 1, pp. 202–208, Feb. 2022.

[28] S. Vellucci, A. Monti, M. Barbuto, A. Toscano, and F. Bilotti, "Progress and perspective on advanced cloaking metasurfaces: From invisibility to intelligent antennas," *EPJ Appl. Metamater.*, vol. 8, p. 7, Jan. 2021.

[29] M. Barbuto et al., "Intelligence enabled by 2D metastructures in antennas and wireless propagation systems," *IEEE Open J. Antennas Propag.*, vol. 3, pp. 135–153, 2022.

[30] A. Alù and N. Engheta, "Achieving transparency with plasmonic and metamaterial coatings," *Phys. Rev. E, Stat. Phys. Plasmas Fluids Relat. Interdiscip. Top.*, vol. 72, no. 1, Jul. 2005, Art. no. 016623.

[31] A. Alù, "Mantle cloak: Invisibility induced by a surface," *Phys. Rev. B, Condens. Matter*, vol. 80, no. 24, Dec. 2009, Art. no. 245115.

[32] A. Monti, J. Soric, A. Alu, F. Bilotti, A. Toscano, and L. Vegni, "Overcoming mutual blockage between neighboring dipole antennas using a low-profile patterned metasurface," *IEEE Antennas Wireless Propag. Lett.*, vol. 11, pp. 1414–1417, 2012.

[33] Z. H. Jiang, P. E. Sieber, L. Kang, and D. H. Werner, "Restoring intrinsic properties of electromagnetic radiators using ultralightweight integrated metasurface cloaks," *Adv. Funct. Mater.*, vol. 25, no. 29, pp. 4708–4716, Aug. 2015.

[34] A. Monti et al., "Mantle cloaking for co-site radio-frequency antennas," *Appl. Phys. Lett.*, vol. 108, no. 11, Mar. 2016, Art. no. 113502.

[35] S. Vellucci, A. Monti, M. Barbuto, A. Toscano, and F. Bilotti, "Satellite applications of electromagnetic cloaking," *IEEE Trans. Antennas Propag.*, vol. 65, no. 9, pp. 4931–4934, Sep. 2017.

[36] H. M. Bernety, A. B. Yakovlev, H. G. Skinner, S.-Y. Suh, and A. Alù, "Decoupling and cloaking of interleaved phased antenna arrays using elliptical metasurfaces," *IEEE Trans. Antennas Propag.*, vol. 68, no. 6, pp. 4997–5002, Jun. 2020.

[37] A. Monti, M. Barbuto, A. Toscano, and F. Bilotti, "Nonlinear mantle cloaking devices for power-dependent antenna arrays," *IEEE Antennas Wireless Propag. Lett.*, vol. 16, pp. 1727–1730, 2017.

[38] S. Vellucci et al., "Non-linear mantle cloaks for self-configurable power-dependent phased arrays," in *Proc. 33rd Gen. Assem. Sci. Symp. Int. Union Radio Sci.*, Aug. 2020, pp. 1–3.

[39] S. Vellucci et al., "On the use of nonlinear metasurfaces for circumventing fundamental limits of mantle cloaking for antennas," *IEEE Trans. Antennas Propag.*, vol. 69, no. 8, pp. 5048–5053, Aug. 2021.

[40] S. Vellucci, A. Monti, M. Barbuto, A. Toscano, and F. Bilotti, "Waveform-selective mantle cloaks for intelligent antennas," *IEEE Trans. Antennas Propag.*, vol. 68, no. 3, pp. 1717–1725, Mar. 2020.

[41] D. Ushikoshi et al., "Pulse-driven self-reconfigurable meta-antennas," *Nature Commun.*, vol. 14, no. 1, p. 633, Feb. 2023.

[42] Z. H. Jiang, M. D. Gregory, and D. H. Werner, "A broadband monopole antenna enabled by an ultrathin anisotropic metamaterial coating," *IEEE Antennas Wireless Propag. Lett.*, vol. 10, pp. 1543–1546, 2011.

[43] S. Vellucci, A. Toscano, F. Bilotti, A. Monti, and M. Barbuto, "Coating metasurfaces enabling antenna frequency reconfigurability for cognitive radio system," in *Proc. IEEE Int. Symp. Antennas Propag. USNC-URSI Radio Sci. Meeting (APS/URSI)*, Dec. 2021, pp. 417–418.

[44] S. Vellucci et al., "Multi-layered coating metasurfaces enabling frequency reconfigurability in wire antenna," *IEEE Open J. Antennas Propag.*, vol. 3, pp. 206–216, 2022.

[45] C. Balanis, *Antenna Theory: Analysis and Design*. Hoboken, NJ, USA: Wiley, 2005.

[46] C. Pfeiffer and A. Grbic, "Metamaterial Huygens' surfaces: Tailoring wave fronts with reflectionless sheets," *Phys. Rev. Lett.*, vol. 110, no. 19, May 2013, Art. no. 197401.

[47] M. Selvanayagam and G. V. Eleftheriades, "Discontinuous electromagnetic fields using orthogonal electric and magnetic currents for wavefront manipulation," *Opt. Exp.*, vol. 21, no. 12, 2013, Art. no. 14409.

[48] A. Monti, A. Alù, A. Toscano, and F. Bilotti, "Surface impedance modeling of all-dielectric metasurfaces," *IEEE Trans. Antennas Propag.*, vol. 68, no. 3, pp. 1799–1811, Mar. 2020.

[49] V. S. Asadchy, M. Albooyeh, S. N. Tcvetkova, A. Díaz-Rubio, Y. Ra'di, and S. A. Tretyakov, "Perfect control of reflection and refraction using spatially dispersive metasurfaces," *Phys. Rev. B, Condens. Matter*, vol. 94, no. 7, 2016, Art. no. 075142.

[50] C. Huygens, *Traité de la Lumiere, Pieter van der Aa*. Amsterdam, The Netherlands: Leyden, 1690.

[51] M. Chen, E. Abdo-Sánchez, A. Epstein, and G. V. Eleftheriades, "Theory, design, and experimental verification of a reflectionless bianisotropic Huygens' metasurface for wide-angle refraction," *Phys. Rev. B, Condens. Matter*, vol. 97, no. 12, Mar. 2018, Art. no. 125433.

[52] A. Epstein and G. V. Eleftheriades, "Huygens' metasurfaces via the equivalence principle: Design and applications," *J. Opt. Soc. Amer. B, Opt. Phys.*, vol. 33, no. 2, p. A31, 2016.

[53] G. A. Egorov and G. V. Eleftheriades, "Theory and simulation of metasurface lenses for extending the angular scan range of phased arrays," *IEEE Trans. Antennas Propag.*, vol. 68, no. 5, pp. 3705–3717, May 2020.

[54] Y.-H. Lv, X. Ding, B.-Z. Wang, and D. E. Anagnostou, "Scanning range expansion of planar phased arrays using metasurfaces," *IEEE Trans. Antennas Propag.*, vol. 68, no. 3, pp. 1402–1410, Mar. 2020.

[55] A. Monti et al., "Quadratic-gradient metasurface-dome for wide-angle beam-steering phased array with reduced gain loss at broadside," *IEEE Trans. Antennas Propag.*, vol. 71, no. 2, pp. 2022–2027, Feb. 2023.

[56] V. G. Ataloglou et al., "Static and reconfigurable Huygens' metasurfaces: Use in antenna beamforming and beam steering," *IEEE Antennas Propag. Mag.*, vol. 64, no. 4, pp. 73–84, Aug. 2022.

[57] D. Ramaccia et al., "Metasurface dome for above-the-horizon grating lobes reduction in 5G-NR systems," *IEEE Antennas Wireless Propag. Lett.*, vol. 21, no. 11, pp. 2176–2180, Nov. 2022.

[58] S. Vellucci, M. Longhi, A. Monti, M. Barbuto, A. Toscano, and F. Bilotti, "Antenna pattern shaping through functionalized metasurface coatings," in *Proc. 16th Int. Congr. Artif. Mater. Novel Wave Phenomena (Metamaterials)*, Sep. 2022, pp. 466–468.

[59] C. Pfeiffer, N. K. Emani, A. M. Shaltout, A. Boltasseva, V. M. Shalaev, and A. Grbic, "Efficient light bending with isotropic metamaterial Huygens' surfaces," *Nano Lett.*, vol. 14, no. 5, pp. 2491–2497, May 2014.

[60] A. Epstein and G. V. Eleftheriades, "Arbitrary power-conserving field transformations with passive lossless omega-type bianisotropic metasurfaces," *IEEE Trans. Antennas Propag.*, vol. 64, no. 9, pp. 3880–3895, Sep. 2016.

[61] D. M. Pozar, *Microwave Engineering*. Hoboken, NJ, USA: Wiley, 2011.

[62] A. Monti et al., "Optimal design of Huygens metasurfaces for oblique incidence through a microwave network approach," in *Proc. Microw. Medit. Symp. (MMS)*, May 2022, pp. 1–4.

[63] D. A. Frickey, "Conversions between S, Z, Y, H, ABCD, and T parameters which are valid for complex source and load impedances," *IEEE Trans. Microw. Theory Techn.*, vol. 42, no. 2, pp. 205–211, Feb. 1994.

[64] G. Bertin, F. Bilotti, B. Piovano, R. Vallauri, and L. Vegni, "Switched beam antenna employing metamaterial-inspired radiators," *IEEE Trans. Antennas Propag.*, vol. 60, no. 8, pp. 3583–3593, Aug. 2012.

[65] R. Harrington, "Reactively controlled directive arrays," *IEEE Trans. Antennas Propag.*, vol. AP-26, no. 3, pp. 390–395, May 1978.

[66] S. Tretyakov, *Analytical Modeling in Applied Electromagnetics*. Norwood, MA, USA: Artech House, 2003.

[67] A. Monti, J. C. Soric, A. Alù, A. Toscano, and F. Bilotti, "Anisotropic mantle cloaks for TM and TE scattering reduction," *IEEE Trans. Antennas Propag.*, vol. 63, no. 4, pp. 1775–1788, Apr. 2015.

[68] C. Qi and A. M. H. Wong, "Discrete Huygens' metasurface: Realizing anomalous refraction and diffraction mode circulation with a robust, broadband and simple design," *IEEE Trans. Antennas Propag.*, vol. 70, no. 8, pp. 7300–7305, Aug. 2022.

Stefano Vellucci (Member, IEEE) received the B.S. and M.S. degrees (summa cum laude) in electronic engineering and the Ph.D. degree in applied electronics from Roma Tre University, Rome, Italy, in 2012, 2015, and 2019, respectively.

In 2014, he joined MBDA, Missile Systems, Rome, as an Intern, and in 2015, he joined ELT Elettronica S.p.A., Rome, as an Antenna Engineer, where he designed, modeled, and optimized antennas for military applications. From 2019 to 2020, he was a Post-Doctoral Researcher with ELEDIA Research Center, University of Trento, Trento, Italy, involved in the study and development of metasurfaces for space and terrestrial applications. From 2020 to 2022, he was a Post-Doctoral Researcher with the Department of Industrial, Electronic, and Mechanical Engineering, Roma Tre University, involved in the development of models and design techniques of reconfigurable metasurfaces for applications in the field of new intelligent antenna systems. Since 2023, he has been with the Department of Engineering, Niccolò Cusano University, Rome as a Post-Doctoral Researcher. His current research interests include the design and applications of artificially engineered materials and metamaterials to RF and microwave components, non-linear and reconfigurable circuit-loaded metasurfaces for radiating structures, analysis, and design of metasurface-based cloaking devices for antennas.

Dr. Vellucci was a recipient of some national and international awards including the URSI Young Scientist Award in 2022, the IEEE AP-S Award of the Central-Southern Italy Chapter in 2019, the Outstanding Reviewers Award assigned by the IEEE TRANSACTIONS ON ANTENNAS AND PROPAGATION from 2018 to 2022, the Leonardo-Finmeccanica Innovation Award for "Young Students" in 2015, and received an Honorary Mention at the "Premio Sorrentino" at the XXIV Riunione Nazionale di Elettromagnetismo (RiNEm) in 2022. He is currently serving as an Associate Editor for the *EPJ Applied Metamaterials* journal, a Guest Editor of two journal special issues focused on microwave, photonic, and mechanical metamaterials, and a member of the Virtual Institute for Artificial Electromagnetic Materials and Metamaterials (METAMORPHOSE VI) and National Inter-University Consortium for Telecommunications (CNIT). In 2019, he was a Local Organizing Committee Member of the International Congress on Artificial Materials for Novel Wave Phenomena—Metamaterials. Since 2016, he has been serving as a Technical Reviewer for many high-level international journals and conferences related to electromagnetic field theory, metamaterial, and metasurfaces.

Michela Longhi (Member, IEEE) received the B.S. and M.S. degrees (summa cum laude) in electronic engineering from Università Politecnica delle Marche, Ancona, Italy, in 2012 and 2014, respectively, and the Ph.D. degree from the University of Tor Vergata, Rome, Italy, in 2019, with European Label.

In 2014, she joined the European Space Agency, Noordwijk, The Netherlands, for the Master thesis project. In 2015, she was a Research Fellow with the Group of Engineering for Health and Wellbeing, Consiglio Nazionale delle Ricerche (CNR-IEIIT), Milan, Italy. In 2019, she was hosted by ETH Zurich, Zürich, Switzerland, for Ph.D., internship. She was an RF and a System Engineer with MVG Italy, Pomezia, Italy, from 2019 to 2021. She is currently a Post-Doctoral Researcher at Niccolò Cusano University, Rome, with the Applied Electromagnetism Laboratory. Her research interests include beam antenna arrays, deep transcranial magnetic investigations, radio frequency identification devices, drones, antennas design, tests, and measurements, and more recently, the synthesis and design of engineered and reconfigurable metasurfaces for antennas also with the support of AI.

Dr. Longhi is a Member of the Italian Society on Electromagnetics (SIEM), National Inter-University Consortium for Telecommunications (CNIT), Virtual Institute for Artificial Electromagnetic Materials and Metamaterials (Metamorphose VI AISBL), IEEE Women in Engineering of the Italian Session (IEEE-WIE), and Inter-University Center for Advanced Studies on Blockchain, Innovation, and Labor Policies (LabChain). She is also a Founder Member of the URSI-Women in Radio Science (URSI-WIRS) Italy Section.

Alessio Monti (Senior Member, IEEE) was born in Rome, Italy, in 1987. He received the B.S. degree (summa cum laude) in electronic engineering, the M.S. degree (summa cum laude) in telecommunications engineering, and the Ph.D. degree in biomedical electronics, electromagnetics, and telecommunications engineering from Roma Tre University, Rome, in 2008, 2010, and 2015, respectively.

From 2013 to 2021, he was with Niccolò Cusano University, Rome, Since November 2021, he has been with the Department of Industrial, Electronic, and Mechanical Engineering, Roma Tre University, where he serves as an Associate Professor in electromagnetic field theory. He is currently the Principal Investigator of the Horizon Europe project "PULSE" focused on reconfigurable plasma metasurfaces (EIC Pathfinder Open project number 10109931) and responsible for a local unit for the project "MANTLES" focused on the use of cloaking metasurfaces for antennas (PRIN 2017 project number 2017BHFZKH). His research activities resulted in more than 130 papers published in international journals, conference proceedings, and book chapters. He has been also involved as a Leader or a Senior Researcher in the activities of more than 30 research projects funded either by national and international bodies or by private companies. His research interests include varied theoretical and application-oriented aspects of metamaterials and metasurfaces at microwave and optical frequencies, the design of functionalized covers and invisibility devices for antennas and antenna arrays, and the electromagnetic modeling of micro- and nano-structured artificial surfaces.

Prof. Monti has been serving with the Scientific Community, by playing important roles in the Editorial Board of International Journals and in the organization of scientific events. In particular, he has been a member of the Secretarial Office of the International Association METAMORPHOSE VI, and of the Editorial Board of the journals *EPJ Applied Metamaterials*, since 2016, and IEEE TRANSACTION ON ANTENNAS AND PROPAGATION, since 2018. In 2019, he was appointed as the General Chair of the International Congress on Artificial Materials for Novel Wave Phenomena—Metamaterials and he has been serving as the Chair of the Steering Committee of the same Congress series, since 2017. He has been also a member of the Technical Program Committee (TPC) of the IEEE International Symposium on Antennas and Propagation (2016–2019) and of the International Congress on Advanced Electromagnetic Materials in Microwaves and Optics-Metamaterials (2014–2016) and has been a Guest-Editor of five journal special issues focused on metamaterials and nanophotonics. He has been a recipient of several national and international awards and recognitions, including the IEEE Senior grade (2019), the URSI Young Scientist Award (2019), the outstanding Associate Editor Award of the IEEE TRANSACTIONS ON ANTENNAS AND PROPAGATION (for four consecutive years, from 2019 to 2022), the Finmeccanica Group Innovation Award for young people (2015), the second place award at the student paper competition of the Metamaterials' conference (2012), and has been selected as a finalist of the student paper competition of IEEE Antennas and Propagation Symposium (2012). He has also been serving as a Technical Reviewer of many high-level international journals related to electromagnetic field theory, metamaterials, and nanophotonics and he has been selected as Top Reviewer by the Editorial Board of the IEEE TRANSACTIONS ON ANTENNAS AND PROPAGATION from 2014 to 2019.

Mirko Barbuto (Senior Member, IEEE) was born in Rome, Italy, in 1986. He received the B.S., M.S., and Ph.D. degrees from "Roma Tre" University, Rome, in 2008, 2010, and 2015, respectively.

Since September 2013, he has been with the "Niccolò Cusano" University, Rome, where he currently serves as an Associate Professor of electromagnetic field theory, as the Director of the Applied Electromagnetic Laboratory, as the Coordinator of the Bachelor's degree in electronic and computer engineering, and as a Member of the Doctoral Board in industrial and civil engineering. He has authored more than 110 papers in international journals and conference proceedings. His main research interests are in the framework of applied electromagnetics, with an emphasis on antennas and components at RF and microwaves, metamaterials and metasurfaces, topological properties of the vortex and composite vortex fields, electromagnetic structures loaded with non-linear or non-foster circuits, and reconfigurable intelligent surfaces (RIS) and smart antennas for wireless systems.

Prof. Barbuto is a member of the Board of Directors and an Institutional Representative within the Virtual Institute for Artificial Electromagnetic Materials and Metamaterials (Metamorphose VI AISBL), and a member of the Scientific Board of the Italian Society on Electromagnetics (SIEM), of the National Inter-University Consortium for Telecommunications (CNIT), and of the Institute of Electrical and Electronics Engineers (IEEE). He is also a member of the Editorial Board of the *Radioengineering Journal*, since 2019 and the Technical Program Committee of the International Congress on Artificial Materials for Novel Wave Phenomena, since 2017. He has been the recipient of the Outstanding Reviewers Awards assigned by the Editorial Board of the IEEE TRANSACTIONS ON ANTENNAS AND PROPAGATION (for eight consecutive years, 2015–2022) and by the Editorial Board of the IEEE ANTENNAS AND WIRELESS PROPAGATION LETTERS (for three consecutive years, 2017–2019). In 2017, he has been selected as one of the Best Reviewers by the Editorial Board of *Radioengineering Journal*. He has been Technical Program Coordinator (Track "Electromagnetics and Materials") for the 2016 IEEE Antennas and Propagation Symposium and he served as Guest Editor of three special issues on metamaterials and metasurfaces. He serves as a Technical Reviewer of the major international conferences and journals related to electromagnetic field theory and metamaterials. Since 2015, he has been the Proceeding Editor for the annual International Congress on Engineered Material Platforms for Novel Wave Phenomena—Metamaterials and, in 2019, he has been appointed as Co-Chair of the 39th EUPROMETA doctoral school on metamaterials held in Rome, Italy. He serves as an Associate Editor for the IEEE TRANSACTIONS ON ANTENNAS AND PROPAGATION since October 2022 and for IEEE ANTENNAS AND WIRELESS PROPAGATION LETTERS since 2019. In 2020 and 2021, he has been awarded for exceptional performance as AE by the board of IEEE AWPL.

Alessandro Toscano (Senior Member, IEEE) was born in Capua, Italy, in 1964. He received the Laurea degree in electronic engineering and the Ph.D. degree from the Sapienza University of Rome, Rome, Italy, in 1988 and 1993, respectively.

Since 2011, he has been a Full Professor of electromagnetic fields with the Engineering Department of Roma Tre University, Rome. He carries out intense academic and scientific activity, both nationally and internationally. From 2013 to 2018, he was a member of Roma Tre University Academic Senate. He has held numerous invited lectures at universities, public and private research institutions, and national and international companies about artificial electromagnetic materials, metamaterials, and their applications. He actively participated in founding the International Association on Metamaterials Virtual Institute for Advanced Electromagnetic Materials—METAMORPHOSE, VI. He coordinates and participates in several research projects and contracts funded by national and international public and private research institutions and industries. He has authored over 150 publications in international journals indexed by ISI or Scopus; of these on a worldwide scale, five are in the first 0.1 percentile, ten in the first 1 percentile, and 25 in the first 5 percentile in terms of the number of quotations and journal quality. His scientific research has as its ultimate objective of conceiving, designing, and manufacturing innovative electromagnetic components with a high technological content that shows enhanced performance compared with those obtained with traditional technologies and that respond to the need for environmental and human health protection. His research activities are focused on three fields: metamaterials and unconventional materials, in collaboration with Professor A. Alù's group at The University of Texas at Austin, Austin, TX, USA.

Prof. Toscano was a Member of the National Commission which enables National Scientific Qualifications to a Full Professor and an Associate Professor in the tender sector 09/F1—electromagnetic fields from 2016 to 2018. From 2018 to 2022, he has been a Vice-Rector for innovation and technology transfer and a Member of the Steering Committee of the National Competence Center on Cyber 4.0. He is currently a member of the Board of Director of Radiolabs and Labchain (non-for-profit Research Consortia), and the Scientific Council of CIRIAF (Interuniversity Research Center on Pollution and the Environment). In addition to his commitment to organizing scientific events, he also carries out an intense editorial activity as a member of the review committees of major international journals and conferences in the field of applied electromagnetics. Research and development of electromagnetic cloaking devices and their applications (First Place Winner of the Leonardo Group Innovation Award for the research project entitled: "Metamaterials and electromagnetic invisibility"), and the research and manufacturing of innovative antenna systems and miniaturized components (First Place Winner of the Leonardo Group Innovation Award for the research project entitled: "Use of metamaterials for miniaturization of components"—MiniMETRIS).

Filiberto Bilotti (Fellow, IEEE) received the Laurea and Ph.D. degrees in electronic engineering from Roma Tre University, Rome, Italy, in 1998 and 2002, respectively.

From 2002 to 2012, he was with the Faculty of Engineering; from 2013 to 2021, he was with the Department of Engineering; and since 2021, he has been with the Department of Industrial, Electronic, and Mechanical Engineering, Roma Tre University, where he has been serving as a Full Professor of electromagnetic field theory, since 2014 and the Director of the Antennas and Metamaterials Research Laboratory since 2012. His main research contributions are in the analysis and design of microwave antennas and arrays, analytical modeling of artificial electromagnetic materials, metamaterials, and metasurfaces, including their applications at both microwave and optical frequencies. In the last ten years, his main research interests have been focused on the modeling and applications of reconfigurable metasurfaces for smart electromagnetic environments, on the development of a new generation of smart antennas based on reconfigurable intelligent surfaces, on gradient and spatially dispersive metasurfaces for dynamic engineering antenna array performances, on space- and time-modulated metasurfaces, on the analysis and design of cloaking metasurfaces for antenna systems, on the topological-based design of antennas supporting structured field, on the concept of metagratings and related applications in optics and at microwaves, and on the modeling and applications of optical metasurfaces. The research activities developed in the last 20 years have resulted in more than 600 articles in international journals, conference proceedings, book chapters, and three patents.

Prof. Bilotti has been serving with the Scientific Community, by playing leading roles in the Management of Scientific Societies, in the Editorial Board of International Journals, and in the organization of conferences and courses. In particular, he was a Founding Member of the Virtual Institute for Artificial Electromagnetic Materials and Metamaterials—METAMORPHOSE VI in 2007. He was elected as a Member of the Board of Directors of the same society for two terms (2007–2013) and as the President for two terms (2013–2019). Currently, he serves the METAMORPHOSE VI as the Vice President and the Executive Director (since 2019). He is a member of the IEEE Antennas and Propagation Meetings Committee since 2022. He was a recipient of a number of awards and recognitions, including elevation to the IEEE Fellow grade for contributions to metamaterials for electromagnetic and antenna applications in 2017, the IEEE Antennas and Propagation Society Chen-To-Tai Distinguished Educator Award in 2023, the Outstanding Associate Editor of the IEEE TRANSACTIONS ON ANTENNAS AND PROPAGATION in 2016, the NATO SET Panel Excellence Award in 2016, the Finmeccanica Group Innovation Prize in 2014, Finmeccanica Corporate Innovation Prize in 2014, the IET Best Poster Paper Award (Metamaterials 2013 and Metamaterials 2011), and the Raj Mittra Travel Grant Senior Researcher Award in 2007. He hosted in 2007 the inaugural edition of the International Congress on Advanced Electromagnetic Materials in Microwaves and Optics—Metamaterials Congress, served as the Chair for the Steering Committee of the same conference for eight editions (2008–2014, 2019), the Chair of the Technical Program Committee (2023), and was elected as the General Chair of the Metamaterials Congress for the period 2015–2018. He was also the General Chair of the Second International Workshop on Metamaterials-by-Design Theory, Methods, and Applications to Communications and Sensing in 2016 and has been serving as the Chair or a Member of the technical program, steering, and organizing committee of the main national and international conferences in the field of applied electromagnetics. He has been serving as an Associate Editor for the IEEE TRANSACTIONS ON ANTENNAS AND PROPAGATION from 2013 to 2017 and, again, from 2022 and the journal *Metamaterials* from 2007 to 2013 and as a member of the Editorial Board of the International Journal on *RF and Microwave Computer-Aided Engineering* from 2009 to 2015, *Nature Scientific Reports* from 2013 to 2016, and *EPJ Applied Metamaterials* since 2013. He was also the guest editor of several special issues in international journals.

Open Access funding provided by 'Università degli Studi Roma Tre' within the CRUI CARE Agreement